CrystEngComm

# An experimental study on polymorph control and continuous heterogeneous crystallization of carbamazepine

| | |
|---|---|
| Journal: | *CrystEngComm* |
| Manuscript ID | CE-ART-06-2019-000908.R1 |
| Article Type: | Paper |
| Date Submitted by the Author: | 02-Jul-2019 |
| Complete List of Authors: | Hu, Chuntian; CONTINUUS Pharmaceuticals,<br>Testa, Christopher; CONTINUUS Pharmaceuticals<br>Shores, Brianna; CONTINUUS Pharmaceuticals<br>Wu, Wei; CONTINUUS Pharmaceuticals<br>Shvedova, Khrystyna; CONTINUUS Pharmaceuticals<br>Born, Stephen; Massachusetts Inst. of Technology, Chemical Engineering; Continuus Pharmaceuticals, Continuus Pharmaceuticals<br>Chattopadhyay, Saptarshi; CONTINUUS Pharmaceuticals<br>Takizawa, Bayan; CONTINUUS Pharmaceuticals<br>Mascia, Salvatore; CONTINUUS Pharmaceuticals |
| | |

CrystEngComm

PAPER

# An experimental study on polymorph control and continuous heterogeneous crystallization of carbamazepine†

Received 00th January 20xx,
Accepted 00th January 20xx

DOI: 10.1039/x0xx00000x

www.rsc.org/

Chuntian Hu,* Christopher J. Testa, Brianna T. Shores, Wei Wu, Khrystyna Shvedova, Stephen C. Born, Saptarshi Chattopadhyay, Bayan Takizawa, and Salvatore Mascia*

Forms I-III and dihydrate carbamazepine (CBZ) were prepared and confirmed by X-ray powder diffraction (XRPD) and differential scanning calorimetry (DSC). Influences of supersaturation ($\sigma$), stirring, anti-solvent ($H_2O$), and polymer type on the resultant polymorph are discussed. For a CBZ ethanol solution at 5 ºC, more than 10 h was required to form crystals when $\sigma$ was 0.5, while less than 2s was required when $\sigma$ was increased to 9.0. Very fine needle-shaped Form II crystals were obtained when $\sigma \geq 7.5$. Higher stirring rates facilitated the formation of Form III CBZ. Continuous heterogeneous crystallization of Form III on Polyvinyl alcohol (PVA, MW 89,000-98,000) was achieved in a one-stage mixed suspension mixed product removal (MSMPR) crystallizer at 15 ºC and 300 rpm. At 5 ºC and 40 rpm, only Form II crystals were obtained. However, Form II CBZ gradually transformed to Form III within 2 residence times, and the transition process was irreversible.

## Introduction

The pharmaceutical industry is transitioning from batch to continuous manufacturing (CM), motivated by the significantly reduced costs and improved quality associated with the latter[1-4]. Orkambi and Prezista tablets have been produced using CM by Vertex Pharmaceuticals and Janssen Pharmaceuticals, respectively[5]. More specifically, they have implemented continuous solutions for their downstream manufacturing processes (*i.e.*, drug product). The end-to-end continuous manufacturing from raw material to final dosage (*i.e.*, integrating drug substance and drug product manufacturing processes) is the next step in this transition, and has already been demonstrated at MIT[6]. A key unit operation in the end-to-end CM of pharmaceuticals is continuous crystallization[5, 7-14], which separates the active pharmaceutical ingredient (API) from the liquid phase and helps with purification prior to downstream processing.

For most small molecule drug products, the final dosage form is a uniform compression or encapsulation of API(s) and excipient(s). After crystallization of the API, subsequent steps (*e.g.*, filtration, drying, milling, blending with excipients, granulation, sieving, tablet pressing, *etc.*) are required[15-19]. As the number of steps increase, so do the challenges, risks, technical hurdles, and considerations[15, 20]. Some steps can be eliminated (*e.g.*, milling, sieving, granulation, *etc.*) if API is directly crystallized on the surface of an excipient within the crystallizer in a continuous crystallization process. This type of crystallization is called continuous heterogeneous crystallization[15, 21].

A common small molecule drug, Carbamazepine (CBZ, 5H-dibenzazepine-5-carboxamide), is used in the treatment of epilepsy and trigeminal neuralgia as a first generation anticonvulsant[22-24]. There are five anhydrous polymorphs of CBZ (*i.e.*, I, II, III, IV, and V), a dihydrate, and several other solvates (*e.g.*, monoacetonate) that have been reported[25-27]. Form V is less common than the other anhydrous polymorphs (Forms I-IV)[23, 26]. Form III (commercially available) is stable below 70 ºC[23, 28], while Forms I, II and IV are metastable. Their stability rank at room temperature is as follows: Form III > Form I > Form IV > Form II[25]; however, Form I becomes the most stable form at temperatures exceeding 130 ºC[29]. Table 1 summarizes Form I-V and dihydrate CBZ data obtained from the literature. Fig. 1 summarizes the polymorphic flow chart, showing the preparation methods and/or the thermal transitions between Forms I-IV CBZ and the dihydrate[25, 30-35].

Polymorphism investigation is important in the pharmaceutical industry because changes between polymorphic forms can lead to changes in properties (*e.g.*, bioavailability and stability of a formulated product)[17, 35-37]. Primary polymorph control factors include supersaturation, temperature, stirring rate, mixing rate of reactant solutions/anti-solvent, and seed crystals[38-42]. Secondary factors include solvent, additives, interface, pH, and host-guest composition, *etc.*[23, 38-40, 43, 44] It is noteworthy that these primary and secondary factors are also dependent on crystallization methods.

*CONTINUUS Pharmaceuticals, 25R Olympia Ave, Woburn, MA, 01801, USA. E-mail: chu@continuuspharma.com; smascia@continuuspharma.com*

† Electronic Supplementary Information (ESI) available. See DOI: 10.1039/x0xx00000x

**Table 1** Summarization of Forms I-V and dihydrate CBZ

| Year | Reference | Form I | Form II | Form III | Form IV | Form V | Dihydrate | Confirmation Method |
|---|---|---|---|---|---|---|---|---|
| 1996 | 34 | Y | – | Y | – | – | Y | XRPD, DSC, FT-Raman, FTIR |
| 2000 | 27 | Y | – | Y | – | – | Y | XRPD, DSC |
| 2002 | 45 | – | – | – | Y | – | – | XRD |
| 2003 | 25 | Y | Y | Y | Y | – | – | XRD, DSC, IR |
| 2004 | 46 | Y | – | Y | – | – | – | FT-Raman |
| 2006 | 33 | Y | – | Y | – | – | – | XRPD |
| 2006 | 35 | Y | Y | Y | – | – | Y | XRD, Raman |
| 2011 | 47 | – | – | Y | – | – | Y | XRPD, DSC, FTIR |
| 2011 | 26 | – | – | – | – | Y | – | XRD |
| 2012 | 29 | – | Y | Y | – | – | – | XRPD |
| 2013 | 24 | – | Y | Y | – | – | – | XRPD |
| 2014 | 48 | Y | – | Y | – | – | Y | XRPD, DSC, |
| 2015 | 49 | – | Y | Y | – | – | – | XRPD |
| 2017 | 40 | – | Y | Y | – | – | – | XRPD |
| 2017 | 23 | – | Y | Y | – | – | – | XRPD |
| 2017 | 50 | Y | Y | Y | – | – | – | XRPD |
| 2017 | 30 | – | – | – | Y | – | – | XRPD, DSC, Raman, |
| 2017 | 5 | – | Y* | Y | – | – | – | XRPD, Raman |
| 2018 | 51 | – | Y* | Y | – | – | – | Raman |
| 2019 | 52 | – | – | Y | – | – | Y | DSC, FT-IR |
| 2019 | This work | Y | Y | Y | – | – | Y | XRPD, DSC |

*Note: The authors believe this is more likely dihydrate CBZ in the presence of water, as demonstrated in Fig. 8

In this work, CBZ Forms I-III and the dihydrate were prepared and compared by X-ray powder diffraction (XRPD) and differential scanning calorimetry (DSC). The impact of supersaturation, stirring, anti-solvent ($H_2O$), and polymer type on the formation of polymorphs is discussed. In addition, experimental results for the continuous heterogeneous crystallization of Forms II/III CBZ on PVA are reported here.

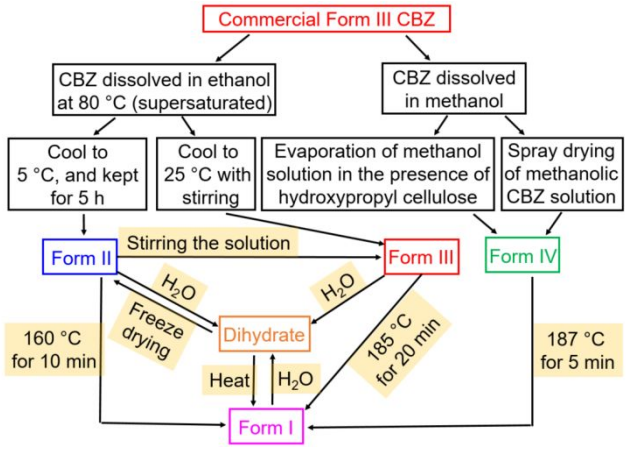


**Fig. 1** Flow chart showing the preparation methods and/or thermal transition between Forms I-IV and the dihydrate CBZ (a combination of methods/conditions used in the current study and references[25, 30-35]).

## Materials and Characterization Methods

### Materials

Commercial CBZ (98%), and anhydrous ethanol were purchased from Fisher Scientific and used as received. Poly (vinyl alcohol) (PVA, MW 13,000-23,000; 85,000-124,000; 89,000-98,000; 146,000-186,000), Poly (Methyl Methacrylate) (PMMA, MW 120,000), Hydroxypropyl Cellulose (HPC, MW 80,000), and Poly Ethylene Oxide (PEO, MW 30,000) were obtained from Sigma-Aldrich. Poly Vinyl Pyrrolidone (PVP, MW 360,000) was purchased from Alfa Aesar.

### X-ray powder diffraction (XRPD)

XRPD measurements were performed using a Miniflex X-ray diffractometer (Rigaku Corporation, Tokyo, Japan). The XRPD was operated under an acceleration voltage of 30 KV and a filament emission of 15 mA. The diffraction patterns were collected over the range of 4-40º (2θ) at a step of 0.02º (2θ).

### Differential scanning calorimetry (DSC)

Thermal analyses of the CBZ samples were performed using a Q20 DSC instrument (TA Instruments, DE, USA). Approximately 5-10 mg of samples were weighted into aluminium pans and sealed. The CBZ samples were equilibrated at 50 ºC, and then heated at a rate of 20 ºC/min over a temperature range of 50-210 ºC under a nitrogen purge of 50 mL/min.

## Results and discussion

### Preparation of anhydrous Forms I-III CBZ

CBZ has four common anhydrous forms, I-IV[25], which makes it an ideal research subject for polymorphism. In this study, anhydrous Forms I-III were prepared following the polymorphic flow chart in Fig. 1. The microscope images of the commercially obtained Form III CBZ and the prepared Forms I-III CBZ are shown in Fig. 2. The morphology of the prepared Forms I-III

CBZ are tiny needle-, needle-, and prismatic-shaped crystals, respectively, which is in agreement with reference data[23, 35]. Form II CBZ was prepared in a 20 mL vial at 5 ºC with supersaturation ($\sigma$) of 2.14 without stirring. The supersaturation was calculated based on the solubility curve of commercial Form III CBZ in ethanol at different temperatures[22] (Fig. 3) with the equation $\sigma=(C-S)/S$, where $C$ and $S$ were the concentration and solubility of CBZ in ethanol at a certain temperature, respectively. In the present study, $\sigma$ was calculated based on the end temperature of a process. Form III CBZ was prepared in a 20 mL vial with stirring under the same supersaturation ($\sigma$=2.14). Form I was prepared through thermal transition, as shown in Fig. 1.

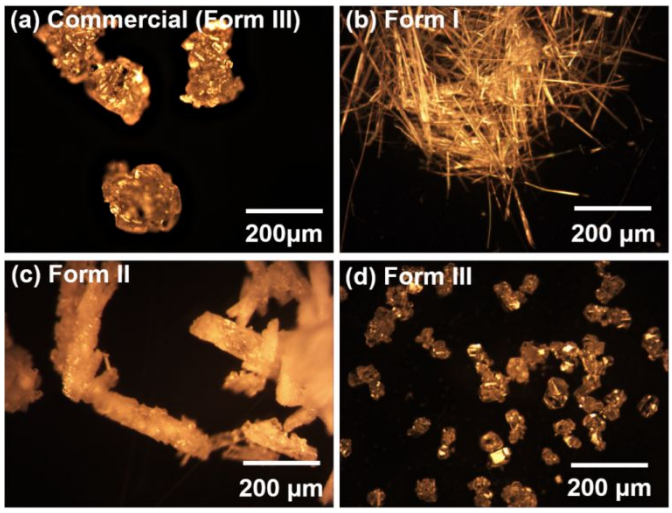


**Fig. 2** Microscope images of (a) commercial Form III, and prepared (b) Form I, (c) Form II, and (d) Form III.

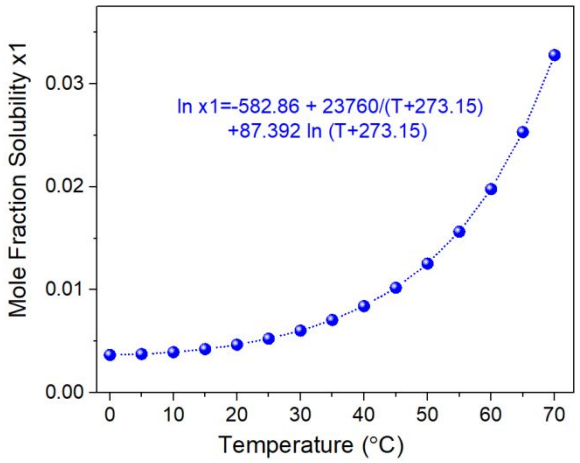


**Fig. 3** Solubility of Form III CBZ in ethanol at temperatures 0-70 °C[22].

Fig. 4a provides the corresponding XRPD of the commercial Form III and the prepared anhydrous Forms I-III CBZ. The characteristic peaks for anhydrous Forms I-III agree well with the values reported[25]. The overall thermal behaviours of commercial Form III and the anhydrous Forms I-III are shown in Fig. 4b. Commercial Form III exhibited a transformation to Form I between 160 and 177 ºC (prepared Form III between 175 and 182 ºC), and the newly generated form (*i.e.*, Form I) melted between 190 and 193 ºC. There was no transformation for prepared Form I before melting. Form II transitioned to Form I between 140 and 160 ºC, and then melted between 190 and 193 ºC.

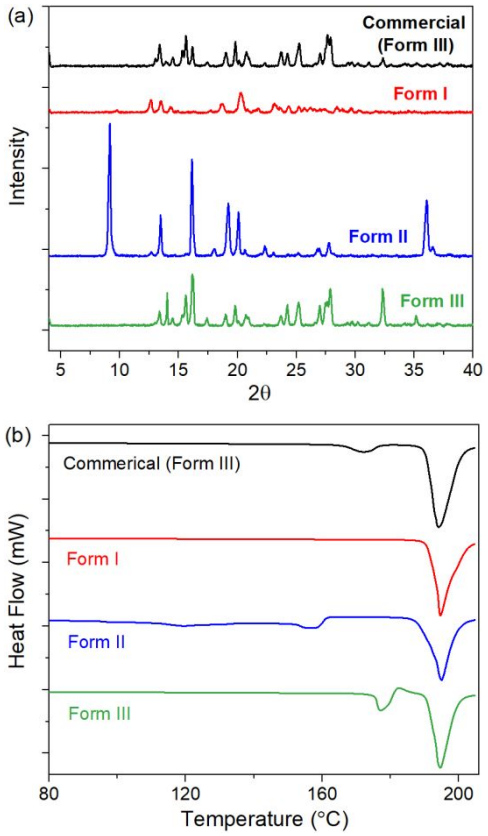


**Fig. 4** (a) XRPD and (b) DSC of the commercial Form III and the prepared anhydrous Forms I-III CBZ samples.

## Impact of supersaturation

Supersaturation ($\sigma$) occurs when a solution contains more solute than its solubility under certain circumstances. It is thermodynamically unstable, and the system is relieved by crystallization. Therefore, supersaturation is a driving force for nucleation and subsequent crystallization. As described above, $\sigma$ was calculated from the solubility curve of commercial CBZ in ethanol at different temperatures[22] (Fig. 3), with the equation of $\sigma=(C-S)/S$. Table 2 shows the influence of $\sigma$ on the onset of nucleation (observed visually). Excess CBZ was dissolved in ethanol in a 20 mL vial at 80 ºC. It was then cooled to 5 ºC in a water bath to induce crystallization (without stirring). When $\sigma$ was 0.5, more than 10 h was required to form crystals, whereas less than 2 s was required when $\sigma$ increased to 9.0.

Fig. 5 illustrates the impact of supersaturation on the morphology of CBZ. Very fine needles were formed when supersaturation $\sigma \geq 7.5$. The reason is that at higher supersaturation ($\sigma \geq 7.5$), crystal nucleation dominates crystal growth, and many more crystal seeds are formed at the onset of

nucleation, which results in the smaller needle size. At low supersaturation, crystal growth is dominant over nucleation, resulting in larger needle size. Fig. 6 shows the XRPD analysis of the CBZ prepared at different $\sigma$, and the characteristic peaks (*e.g.*, 8.7º) indicate that Form II CBZ is obtained for $\sigma$ of 1.5, 2.14, 7.5 and 9.0, and mixture of Form II and III CBZ is obtained for $\sigma$ of 4.5 and 6.0.

**Table 2** Influence of supersaturation on the onset of nucleation

| Sample # | Supersaturation (σ) | Nucleation onset |
|---|---|---|
| 1 | 0.5 | > 10 h |
| 2 | 1.5 | 2-3 h |
| 3 | 2.14 | 10-40 min |
| 4 | 4.5 | 4-6 min |
| 5 | 6.0 | 1-3 min |
| 6 | 7.5 | 10-30 s |
| 7 | 9.0 | < 2 s |

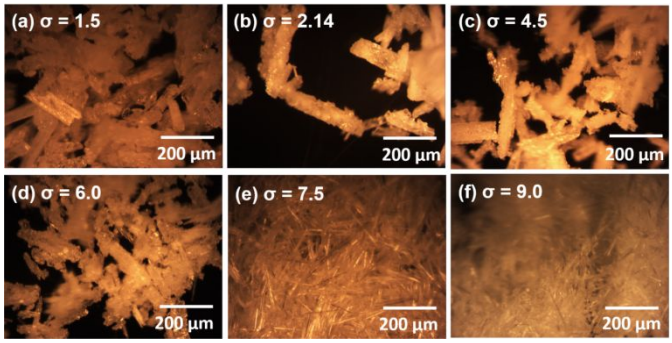


**Fig. 5** Microscope images of CBZ formed under different supersaturation.

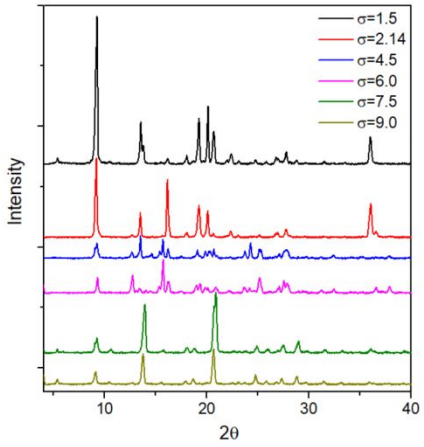


**Fig. 6** XRPD of CBZ prepared at different supersaturation conditions.

### Impact of stirring and antisolvent

Formation of a specific crystal polymorph is determined by the relative kinetics of nucleation and its subsequent growth, which is highly influenced by stirring. To investigate the impact of stirring, 19 mL CBZ ethanol solutions with $\sigma$ = 2.14 were prepared and dissolved in 20 mL vials at 80 ºC. The vials were then cooled and maintained at 5 ºC in a water bath for 5h. Without stirring, needle-shaped Form II crystals were obtained (Fig. 7a) at t= 5 h (onset time was 10-40 min, samples were taken at 5 h) as confirmed by XRPD (Fig. 7c) and DSC (Fig. 7d). However, after several days, the needle crystals gradually transformed to prismatic-shaped Form III CBZ. At a stirring rate of 300 rpm, a clear onset of turbidity was observed within 2 min. Prismatic-shaped crystals of Form III were obtained (Fig. 7b), which was also confirmed by XRPD and DSC (Fig. 7c-d).

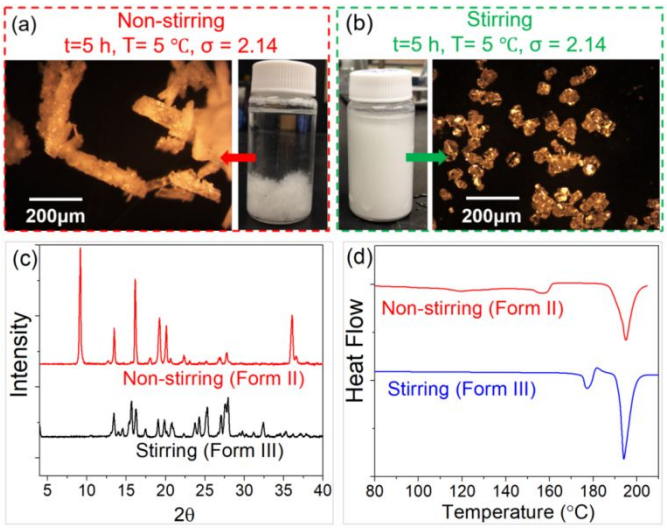


**Fig. 7** Influence of stirring on polymorph of CBZ: (a) Form II without stirring, (b) Form III with stirring, (c) XRPD and (d) DSC of the non-stirring and stirring samples.

It is well known that commercial Form III CBZ (solid powder) is hygroscopic, and Form III CBZ transforms to the dihydrate CBZ after absorbing $H_2O$[48]. Under stirring conditions, the addition of $H_2O$ (as anti-solvent) in CBZ ethanol solution was investigated. A 9 mL CBZ ethanol solution with $\sigma$ = 2.14 was prepared and dissolved in a 20 mL vial at 80 ºC. The vial was then cooled and maintained at 5 ºC. After stirring for 1 h, Form III CBZ was obtained. Different amounts of $H_2O$ (ranged from 5 to 75 vol%) were then added and stirred at 300 rpm. For water concentration of 5 and 10 vol%, mainly prismatic-shaped crystals were obtained (Fig. 8a-b) and only very few needle crystals were observed. The XRPD and DSC analysis showed that Form III crystals were obtained (Fig. 8g-h for 5 and 10 vol% samples). When water concentration was 15 vol% or higher, the Form III CBZ gradually transformed to dihydrate CBZ, which has needle-shaped crystals (Fig. 8c-f). Fig. 8g shows the XRPD of the dihydrate CBZ sample (for water concentration ≥ 15 vol%) and the specific peaks of 8.9, 12.3 and 18.6º, which agree well with the literature data[35, 48]. Fig. 8h provides DSC results of the dihydrate CBZ (for water concentration ≥ 15 vol%), which confirms the formation of dihydrate CBZ[47]. There are two endothermic peaks at 90-120 ºC that correspond to the dehydration of the dihydrate CBZ, and the subsequent evaporation of $H_2O$. In this heating process, dihydrate CBZ lost $H_2O$, and ultimately transformed to Form I CBZ.

Similarly, no transition from Form III to dihydrate CBZ was observed when crystallization occurred directly in the ethanol-

water solution for water concentration of 5 and 10 vol%. When water concentration was greater than 15 vol%, CBZ crystallized out as dihydrate instead of Form III. As an example, 9 mL CBZ ethanol solution with $\sigma = 2.14$ was prepared in a 20 mL vial. 9 mL $H_2O$ was then added and stirred at 300 rpm, and the mixture was heated at 80 ºC for dissolution. The dissolved solution was then maintained at 5 ºC under stirring. Crystallization occurred and the obtained crystals were analysed using XRPD and DSC. The results showed that dihydrate CBZ was obtained.

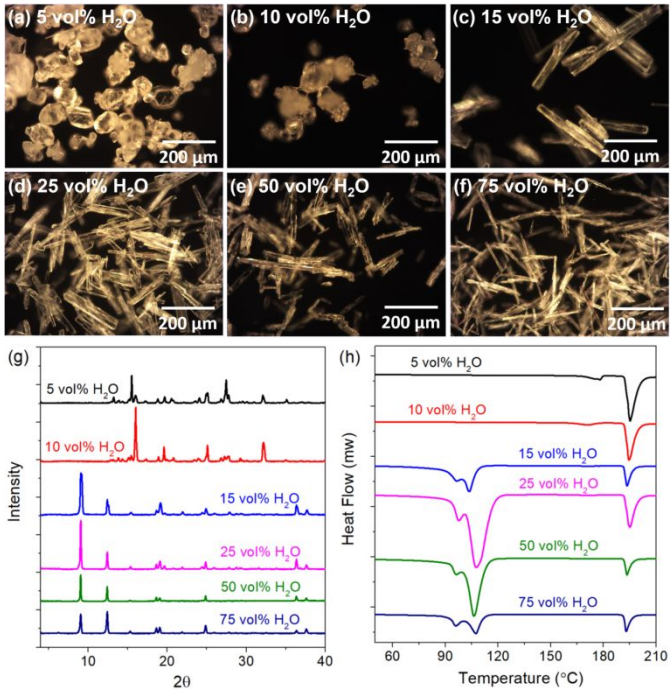


**Fig. 8** (a-f) Microscope images of the Form III/dihydrate CBZ prepared in an ethanol-water solution, and the relevant (g) XRPD, and (h) DSC.

### Impact of polymer type

For the CBZ system, the introduction of foreign surfaces can influence the polymorph and morphology outcomes. For example, it has been shown that the stable Form III nucleates on tin, while the metastable Form II nucleates on glass and PTFE[23]. The influence of several polymers on CBZ polymorph formation in ethanol solution ($\sigma = 2.14$) was investigated and the results summarized in Table 3. With a stirring rate of 300 rpm, only Form III was observed, at both 5 and 25 ºC (ending temperature). Without stirring, only Form II was obtained at 5 ºC. However, at 25 ºC, both Forms II and III were observed in the presence of PVA (MW 89,000-98,000), HPC, and PEO. Only Form III was obtained in the presence of the other polymers (*i.e.*, PVA (MW 85,000-124,000), PVA (MW 146,000-186,000), PVA (MW 13,000-23,000), PVP and PMMA).

**Table 3** Influence of polymer type on polymorphs of CBZ

| Polymer | Molecular Weight | Non-stirring | | Stirring | |
|---|---|---|---|---|---|
| | | 5ºC | 25ºC | 5ºC | 25ºC |
| 1. PVA | 85,000-124,000 | II | III | III | III |
| 2. PVA | 146,000-186,000 | II | III | III | III |
| 3. PVA | 13,000-23,000 | II | III | III | III |
| 4. PVA | 89,000-98,000 | II | II&III | III | III |
| 5. PVP | 360,000 | II | III | III | III |
| 6. PMMA | 120,000 | II | III | III | III |
| 7. HPC | 80,000 | II | II&III | III | III |
| 8. PEO | 30,000 | II | II&III | III | III |

Fig. 9 shows the polymorph of CBZ in the presence of PVA (MW 89,000-98,000). Without stirring, CBZ crystallized as a combination of needle-shaped CBZ in the bulk (Fig. 9a-b) and prismatic-shaped crystals on the surface of the PVA (Fig. 9b). At a stirring rate of 300 rpm, CBZ crystallized as prismatic-shaped Form III CBZ on the polymer surface (Fig. 9c), and no needle-shaped crystals were observed. After heating the stirring samples at 160 ºC for 1 h, tiny needle-shaped Form I CBZ was observed (Fig. 9d). The corresponding XRPD results of the samples in Fig. 9a-d are shown in Fig. 9e.

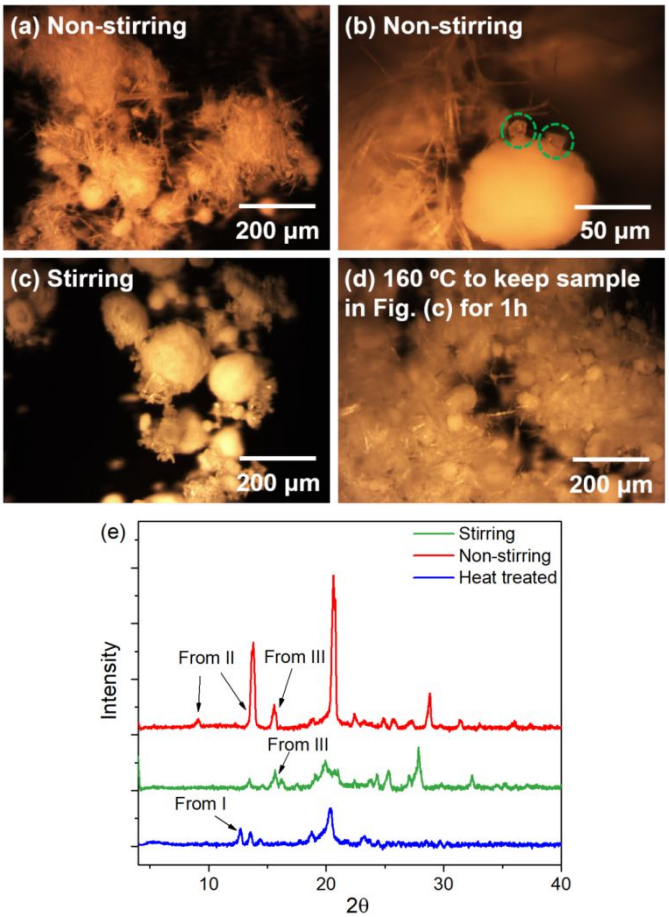


**Fig. 9** Polymorph of CBZ in the presence of PVA (MW 89,000-98,000): (a) and (b) non-stirring, (c) stirring, (d) heat treated (160 ºC for 1 h) stirring samples, and the relevant (e) XRPD.

**Continuous heterogeneous crystallization**

Continuous heterogeneous crystallization could eliminate certain manufacturing steps, such as milling, sieving, granulation *etc*. Fig. 10 shows the process flow diagram of a one-stage mixed suspension mixed product removal (MSMPR) heterogeneous crystallization system. A CBZ ethanol solution with $\sigma = 2.14$ was prepared in a dissolution vessel at 80 ºC and 300-500 rpm. When the crystallization vessel was maintained at 15 ºC and 300 rpm, continuous heterogeneous crystallization of prismatic-shaped Form III CBZ on the PVA (MW 89,000-98,000) surface was achieved (Fig. 11a). When the crystallization vessel was maintained at 5 ºC and 50 rpm, both needle-shaped Form II CBZ (both in bulk and on the polymer surface) and prismatic-shaped Form III CBZ (on the polymer surface) were observed (Fig. 11b) at t= 5 min. When the stirring rate decreased to 40 rpm (PVA settling was observed), only needle-shaped Form II CBZ was observed both on the PVA surface and in the bulk (Fig. 11c) at t=5 min. However, Form II CBZ gradually transformed to Form III in the crystallization vessel, and the bulk crystals gradually grew on the polymer surface (Fig. 11c-f). The transition was completed within 2.5 h (~ 2 residence times). Additionally, prismatic-shaped Form III CBZ was easier to grow on the PVA (MW 89,000-98,000) surface than was the needle-shaped Form II CBZ, which was more likely to crystallize in bulk.

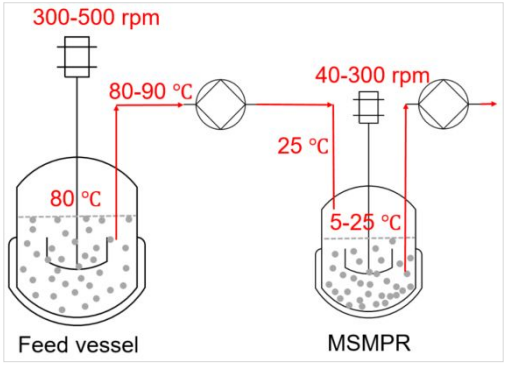


**Fig. 10** Process flow diagram of the one-stage MSMPR crystallizer.

The ideal solubility of Form II or Form III CBZ in ethanol at T (°C) can be estimated using the following equation[53, 54]:

$$x_j(T) = \exp\left(-\frac{\overline{\Delta H_j^f}}{R(T_j^f + 273.15)}\, ln\left(\frac{T_j^f + 273.15}{T + 273.15}\right)\right) \qquad (1)$$

where $x_j(T)$ is the mole fraction solubility of CBZ Form j (j=II, III), $\overline{\Delta H_j^f}$ is the molar enthalpy of fusion of CBZ Form j at its melting point, R is the ideal gas constant, $T_j^f$ is the melting point of CBZ Form j. According to the present study and literature value[25], $\overline{\Delta H_{II}^f} = 23.94$ kJ/mol, $\overline{\Delta H_{III}^f} = 26.83$ kJ/mol, $T_{II}^f = 140$ °C, and $T_{III}^f = 175$ °C. The ideal solubility ratio of CBZ Form II to Form III from 0-70 °C is calculated to be ~ 1.8, which is higher than the reported experimental value of ~ 1.1 in the literature[23, 49]. However, equation (1) is still a useful tool to estimate the solubility of metastable polymorphs in most cases[54, 55]. Obviously, Form II CBZ has a higher solubility than Form III. As the system strives to achieve equilibrium, Form II CBZ crystals dissolve and recrystallize as Form III characterized by a lower solubility.

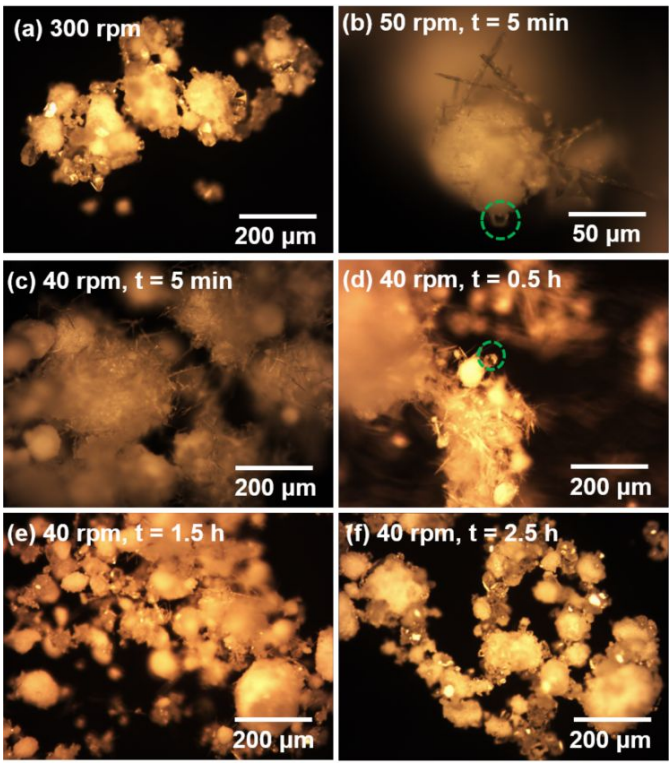


**Fig. 11** Microscope images of heterogeneous crystallization of CBZ on the surface of PVA particles in the one-stage MSMPR.

Low stirring rates, (<50 rpm, or non-stirring) and low temperatures (4-5 ºC) facilitate the formation of Form II CBZ. Therefore, a plug flow crystallizer was used as shown in Fig. S1 (see ESI†). The feed was heated to 80 ºC, and then pumped into 20 feet long 2/32 inch ID tubing, which was immersed in a 5 ºC liquid bath. The residence time in the tubing was approximately 20-30 min. The crystals were then filtered using a batch vacuum filtration unit, and a mixture of Form II and Form III was obtained (Fig. S2). Clogging was encountered in experiments that included PVA (MW 89,000-98,000).

One challenge for this process is that the transition from Form II to Form III is irreversible. To prevent this transition, a different reactor design to prevent clogging, anti-solvents to change the solubility ratio, or additives may be implemented and/or added. Water is not a good choice for an anti-solvent in the present case because: 1) PVA is soluble in water, and 2) dihydrate CBZ is obtained instead of Form II. Besides polymorph control, further studies, such as drug loading and avoidance of bulk nucleation, are needed to achieve a robust continuous heterogeneous crystallization solution.

## Conclusions

A flow chart showing the preparation methods and/or thermal transition between Forms I-IV and the dihydrate CBZ was summarized in the present study. Anhydrous Forms I-III were prepared following this polymorphic flow chart, and confirmed by XRPD and DSC analysis. From the DSC data, commercial Form III, prepared Forms II and III transformed to Form I at 160-177 ºC, 140-160 ºC, and 175-182 ºC, respectively.

Supersaturation plays an important role in the nucleation and crystallization, as well as polymorph and morphology[38]. For a CBZ ethanol solution at 5 ºC, when supersaturation $\sigma$ was 0.5, more than 10 h was required to form crystals, while less than 2s was required when $\sigma$ increased to 9.0. Very fine needle-shaped crystals were formed when $\sigma \geq 7.5$.

Stirring greatly influences the formation of certain polymorphs. For a CBZ ethanol solution with $\sigma$ =2.14 at 5 ºC, needle-shaped Form II crystals were obtained without stirring. With stirring at 300 rpm, a clear onset of turbidity was observed within 2 min, and Form III was obtained. After adding $H_2O$ greater than 15 vol%, Form III gradually transformed to dihydrate CBZ, which was confirmed by XRPD and DSC. The dihydrate CBZ had specific peaks of 8.9, 12.3 and 18.6º, and dehydrated between 90-102 ºC.

The introduction of foreign surfaces (*i.e.*, PVA, PVP, PMMA, HPC, and PEO) clearly impacted polymorph and morphology outcomes for the CBZ system (ethanol solution with $\sigma$ = 2.14). With a stirring rate of 300 rpm, only Form III was observed, both at 5 and 25 ºC. Without stirring, only Form II was obtained at 5 ºC. However, at 25 ºC, both Form II and III were observed in the presence of PVA (MW 89,000-98,000), HPC and PEO.

With continuous heterogeneous crystallization, API is crystallized directly on the surface of an excipient within the continuous crystallizer, which could eliminate certain manufacturing steps, such as milling, sieving, and granulation. Continuous heterogeneous crystallization of Form III CBZ on PVA (MW 89,000-98,000) was achieved at 15 ºC and 300 rpm in a one-stage MSMPR. When the stirring rate decreased to 40 rpm, only Form II CBZ was obtained at 5 ºC. However, Form II CBZ gradually transformed to Form III within 2 residence times, and the transition process was irreversible.

## Conflicts of interest

There are no conflicts to declare.

## Acknowledgements

This work has been supported by the NSF SBIR under Award # 1555647.

## References

1. S. D. Schaber, D. I. Gerogiorgis, R. Ramachandran, J. M. Evans, P. I. Barton and B. L. Trout, *Industrial & Engineering Chemistry Research*, 2011, **50**, 10083-10092.
2. K. Plumb, *Chemical Engineering Research and Design*, 2005, **83**, 730-738.
3. P. McKenzie, S. Kiang, J. Tom, A. E. Rubin and M. Futran, *AIChE Journal*, 2006, **52**, 3990-3994.
4. C. Hu, J. E. Finkelstein, W. Wu, K. Shvedova, C. J. Testa, S. C. Born, B. Takizawa, T. F. O'Connor, X. Yang and S. Ramanujam, *Reaction Chemistry & Engineering*, 2018, **3**, 658-667.
5. X. Yang, D. Acevedo, A. Mohammad, N. Pavurala, H. Wu, A. L. Brayton, R. A. Shaw, M. J. Goldman, F. He and S. Li, *Organic Process Research & Development*, 2017, **21**, 1021-1033.
6. S. Mascia, P. L. Heider, H. Zhang, R. Lakerveld, B. Benyahia, P. I. Barton, R. D. Braatz, C. L. Cooney, J. Evans and T. F. Jamison, *Angewandte Chemie International Edition*, 2013, **52**, 12359-12363.
7. S. Lawton, G. Steele, P. Shering, L. Zhao, I. Laird and X.-W. Ni, *Organic Process Research & Development*, 2009, **13**, 1357-1363.
8. A. Randolph, *Theory of particulate processes: analysis and techniques of continuous crystallization*, Elsevier, 2012.
9. S. Y. Wong, A. P. Tatusko, B. L. Trout and A. S. Myerson, *Crystal Growth & Design*, 2012, **12**, 5701-5707.
10. J. L. Quon, H. Zhang, A. Alvarez, J. Evans, A. S. Myerson and B. L. Trout, *Crystal Growth & Design*, 2012, **12**, 3036-3044.
11. H. Zhang, J. Quon, A. J. Alvarez, J. Evans, A. S. Myerson and B. Trout, *Organic Process Research & Development*, 2012, **16**, 915-924.
12. O. Narducci, A. Jones and E. Kougoulos, *Chemical engineering science*, 2011, **66**, 1069-1076.
13. H. Zhang, R. Lakerveld, P. L. Heider, M. Tao, M. Su, C. J. Testa, A. N. D'Antonio, P. I. Barton, R. D. Braatz and B. L. Trout, *Crystal Growth & Design*, 2014, **14**, 2148-2157.
14. A. J. Alvarez and A. S. Myerson, *Crystal Growth & Design*, 2010, **10**, 2219-2228.
15. N. Yazdanpanah, C. J. Testa, S. R. Perala, K. D. Jensen, R. D. Braatz, A. S. Myerson and B. L. Trout, *Crystal Growth & Design*, 2017, **17**, 3321-3330.
16. K. Chadwick, J. Chen, A. S. Myerson and B. L. Trout, *Crystal Growth & Design*, 2012, **12**, 1159-1166.
17. K. Chadwick, A. Myerson and B. Trout, *CrystEngComm*, 2011, **13**, 6625-6627.
18. J. L. Quon, K. Chadwick, G. P. Wood, I. Sheu, B. K. Brettmann, A. S. Myerson and B. L. Trout, *Langmuir*, 2013, **29**, 3292-3300.
19. Y. Diao, A. S. Myerson, T. A. Hatton and B. L. Trout, *Langmuir*, 2011, **27**, 5324-5334.
20. M. Sharma and B. L. Trout, *The Journal of Physical Chemistry B*, 2015, **119**, 8135-8145.
21. V. Verma, R. V. Peddapatla, C. M. Crowley, A. M. Crean, P. Davern, S. Hudson and B. K. Hodnett, *Crystal Growth & Design*, 2017, **18**, 338-350.
22. W. Liu, L. Dang, S. Black and H. Wei, *Journal of Chemical & Engineering Data*, 2008, **53**, 2204-2206.
23. H. Yang, C. L. Song, Y. X. Lim, W. Chen and J. Y. Heng, *CrystEngComm*, 2017, **19**, 6573-6578.
24. W. Liu, H. Wei, J. Zhao, S. Black and C. Sun, *Organic Process Research & Development*, 2013, **17**, 1406-1412.
25. A. L. Grzesiak, M. Lang, K. Kim and A. J. Matzger, *Journal of pharmaceutical sciences*, 2003, **92**, 2260-2271.
26. J.-B. Arlin, L. S. Price, S. L. Price and A. J. Florence, *Chemical Communications*, 2011, **47**, 7074-7076.
27. Y. Kobayashi, S. Ito, S. Itai and K. Yamamoto, *International journal of pharmaceutics*, 2000, **193**, 137-146.
28. R. J. Behme and D. Brooke, *Journal of pharmaceutical sciences*, 1991, **80**, 986-990.
29. K. Sypek, I. S. Burns, A. J. Florence and J. Sefcik, *Crystal Growth & Design*, 2012, **12**, 4821-4828.
30. R. A. Halliwell, R. M. Bhardwaj, C. J. Brown, N. E. Briggs, J. Dunn, J. Robertson, A. Nordon and A. J. Florence, *Journal of pharmaceutical sciences*, 2017, **106**, 1874-1880.
31. K. Kipouros, K. Kachrimanis, I. Nikolakakis and S. Malamataris, *Analytica chimica acta*, 2005, **550**, 191-198.
32. K. Kipouros, K. Kachrimanis, I. Nikolakakis, V. Tserki and S. Malamataris, *Journal of pharmaceutical sciences*, 2006, **95**, 2419-2431.
33. F. Tian, D. J. Saville, K. C. Gordon, C. J. Strachan, J. A. Zeitler, N.

Sandler and T. Rades, *Journal of pharmacy and pharmacology*, 2007, **59**, 193-201.
34. L. E. McMahon, P. Timmins, A. C. Williams and P. York, *Journal of pharmaceutical sciences*, 1996, **85**, 1064-1069.
35. F. Tian, J. Zeitler, C. Strachan, D. Saville, K. Gordon and T. Rades, *Journal of Pharmaceutical and Biomedical Analysis*, 2006, **40**, 271-280.
36. L. Nicoud, F. Licordari and A. S. Myerson, *CrystEngComm*, 2019, **21**, 2105-2118.
37. L. Nicoud, F. Licordari and A. S. Myerson, *Organic Process Research & Development*, 2019.
38. M. Kitamura, *CrystEngComm*, 2009, **11**, 949-964.
39. A. Llinàs and J. M. Goodman, *Drug Discovery Today*, 2008, **13**, 198-210.
40. J. V. Parambil, S. K. Poornachary, R. B. Tan and J. Y. Heng, *Journal of Crystal Growth*, 2017, **469**, 84-90.
41. C. Sudha and K. Srinivasan, *CrystEngComm*, 2013, **15**, 1914-1921.
42. M. Kitamura, *Journal of Crystal Growth*, 2002, **237**, 2205-2214.
43. P. Christian, C. Röthel, M. Tazreiter, A. Zimmer, I. Salzmann, R. Resel and O. Werzer, *Crystal growth & design*, 2016, **16**, 2771-2778.
44. M. Lang, A. L. Grzesiak and A. J. Matzger, *Journal of the American Chemical Society*, 2002, **124**, 14834-14835.
45. M. Lang, J. W. Kampf and A. J. Matzger, *Journal of pharmaceutical sciences*, 2002, **91**, 1186-1190.
46. L. E. O'brien, P. Timmins, A. C. Williams and P. York, *Journal of pharmaceutical and biomedical analysis*, 2004, **36**, 335-340.
47. Z. Rahman, C. Agarabi, A. S. Zidan, S. R. Khan and M. A. Khan, *Aaps Pharmscitech*, 2011, **12**, 693-704.
48. M. A. L. Pinto, B. Ambrozini, A. P. G. Ferreira and É. T. G. Cavalheiro, *Brazilian Journal of Pharmaceutical Sciences*, 2014, **50**, 877-884.
49. J. V. Parambil, S. K. Poornachary, S. J. Hinder, R. B. Tan and J. Y. Heng, *CrystEngComm*, 2015, **17**, 6384-6392.
50. L. Padrela, J. Zeglinski and K. M. Ryan, *Crystal Growth & Design*, 2017, **17**, 4544-4553.
51. D. Acevedo, X. Yang, A. Mohammad, N. Pavurala, W.-L. Wu, T. F. O'Connor, Z. K. Nagy and C. N. Cruz, *Organic Process Research & Development*, 2018, **22**, 156-165.
52. S. F. B. Ali, Z. Rahman, S. Dharani, H. Afrooz and M. A. Khan, *Journal of pharmaceutical sciences*, 2019, **108**, 1211-1219.
53. S. H. Neau, S. V. Bhandarkar and E. W. Hellmuth, *Pharmaceutical research*, 1997, **14**, 601-605.
54. L. Nicoud, F. Licordari and A. S. Myerson, *Crystal Growth & Design*, 2018, **18**, 7228-7237.
55. C. Mao, R. Pinal and K. R. Morris, *Pharmaceutical research*, 2005, **22**, 1149-1157.

 